Available online at www.sciencedirect.com

SciVerse ScienceDirect

Journal of the European Ceramic Society 32 (2012) 2739–2746

www.elsevier.com/locate/jeurceramsoc

# Structural and thermal characterization of $CaO–MgO–SiO_2–P_2O_5–CaF_2$ glasses

Ishu Kansal [a], Ashutosh Goel [b], Dilshat U. Tulyaganov [c], Raghu Raman Rajagopal [a], José M.F. Ferreira [a,*]

[a] *Department of Ceramics and Glass Engineering, University of Aveiro, CICECO, 3810- 193 Aveiro, Portugal*
[b] *Pacific Northwest National Laboratory, Richland, WA 99354, USA*
[c] *Turin Polytechnic University in Tashkent, 100174 Tashkent, Uzbekistan*

Available online 21 November 2011

**Abstract**

The influence of varying the CaO/MgO ratio on the structure and thermal properties of $CaO–MgO–SiO_2–P_2O_5–CaF_2$ glasses was studied in a series of eight glass compositions in the glass forming region of diopside ($CaMgSi_2O_6$)–fluorapatite [$Ca_5(PO_4)_3F$]–wollastonite ($CaSiO_3$) ternary system. The melt-quenched glasses were characterized for their structure by infrared spectroscopy (FTIR) and magic angle spinning (MAS)-nuclear magnetic resonance (NMR) spectroscopy. Silicon is predominantly present as $Q^2$ (Si) species, while phosphorus tends to coordinate in orthophosphate environment. The sintering and crystallization parameters of the glasses were obtained from differential thermal analysis (DTA) while crystalline phase fractions in the sintered glass–ceramics were analyzed by X-ray diffraction adjoined with Rietveld refinement. Diopside, fluorapatite, wollastonite and pseudowollastonite crystallized as the main crystalline phases in all the glass–ceramics with their content varying with respect to variation in CaO/MgO ratio in glasses. The implications of structure and sintering behaviour of glasses on their bioactivity were discussed.
Published by Elsevier Ltd.

*Keywords:* A. Sintering; C. Thermal properties; D. Glass; D. Glass–ceramics; E. Biomedical applications

## 1. Introduction

The concept of bioactive ceramics was introduced by Hench et al.[1] This led to a standard definition of bioactivity, "a bioactive material is the one which elicit a special response on its surface when in contact with biological fluids, leading to strong bonding to living tissue".[1] In the field of bone engineering, bioactivity is defined as the ability of a material to bond to bone tissue *via* the formation of a bone-like hydroxyapatite layer on its surface.[2] Bioactive materials have been classified in two different sets namely, 'Class A' and 'Class B'. Class A bioactivity is 'the process whereby a biological surface is colonized by osteogenic stem cells free in the defect environment as a result of surgical intervention'. An extra- as well as intracellular response is elicited by a 'Class A' bioactive material at the interface. Such materials are said to be osteoproductive. 'Class B' bioactivity is a bioinductive pathway that allows bone to grow along it, thus, the material only exhibits an extracellular response at the interface. Such materials are known as osteoconductive.[2] Bioactive glasses and glass–ceramics are typical examples of 'Class A' biomaterials.

A paradigm shift is taking place in the field of biomaterials from using synthetic implants and tissue grafts to a tissue engineering approach that uses porous material scaffolds integrated with biological cells or molecules to regenerate tissues.[3] Therefore, this new paradigm requires scaffolds that balance temporary mechanical function with mass transport to aid biological delivery and tissue regeneration in three dimensions (3D).[4] Further, when using a synthetic scaffold, its use should be as short lived as possible; at the same time the scaffold must maintain its viability and integrity long enough for the cells to produce their own extracellular matrix. Therefore, a major consideration when designing a scaffold for tissue engineering is the scaffold material.

Bioactive glass–ceramics are ideal materials for scaffold fabrication owing to their ease of processing, good sintering ability and mechanical strength and high bioactivity.[5–8]

* Corresponding author. Tel.: +351 234 370242; fax: +351 234 370204.
*E-mail addresses:* ashutosh.goel@pnnl.gov (A. Goel), jmf@ua.pt (J.M.F. Ferreira).

0955-2219/$ – see front matter. Published by Elsevier Ltd.
doi:10.1016/j.jeurceramsoc.2011.10.041

The glass–ceramics in the diopside ($CaMgSi_2O_6$)–fluorapatite [$Ca_5(PO_4)_3F$]–wollastonite ($CaSiO_3$) system are potential candidates for scaffold fabrication for bone tissue engineering. Shibuya et al.[9] developed non-alkali-containing diopside–fluorapatite–wollastonite bioactive glass–ceramics for replacement materials for tooth roots, dental crowns and bones. Similarly, Salman et al.[10] studied the *in vitro* bioactivity of diopside–fluorapatite–wollastonite–sodium silicate-based glass–ceramics by immersion in simulated body fluid. The as-prepared and investigated glass–ceramics exhibited excellent bioactivity and were proposed to be suitable for restorative dental and bone implants materials. Recently, Kansal et al.[5] investigated the structural and thermal behaviour of diopside–fluorapatite–wollastonite based glasses and glass–ceramics with varying $CaO/SiO_2$ and $CaF_2/P_2O_5$ ratios, respectively.

The present study aims at investigating the sintering behaviour of glasses designed in ternary system of diopside–fluorapatite–wollastonite with varying diopside/wollastonite ratio while maintaining constant fluorapatite content (20 wt.%). The parent glass–ceramic composition in this study (i.e. 80% diopside–20% fluorapatite) derives from our previous investigation pertaining to diopside–fluorapatite glass–ceramics[11] where the potential of this composition in bone tissue engineering has been successfully demonstrated. Therefore, this study is an attempt to improve the sintering ability and bioactivity of these glass–ceramics by substituting diopside with wollastonite. Although, diopside[12,13] as well as wollastonite[14,15] are proven biomaterials but still substituting diopside with wollastonite is expected to enhance the bioactivity of resultant glass–ceramics owing to the high chemical degradability of latter.[15] It should be noted that this paper will focus only on the structure and thermal properties of these glasses while the biological studies on these glasses and resultant glass–ceramics will be reported in our forthcoming article. Table 1 presents the compositions of the investigated glasses. As is evident from Table 1, varying diopside/wollastonite ratio in glasses basically varies the MgO/CaO ratio in glasses. Therefore, further discussion of results pertaining to characterization of glasses will be based on the increase in CaO/MgO ratio in glasses corresponding to increasing wollastonite/diopside ratio.

## 2. Experimental

### 2.1. Synthesis of glasses

A series of glass compositions in the system $[CaMgSi_2O_6]_{80-x}$ $[Ca_5(PO_4)_3F]_{20}$–$[CaSiO_3]_x$ ($x$ = 10–80 wt.%) have been prepared with varying diopside/wollastonite ratios by melt-quenching technique. The glass compositions were labelled in accordance with the wollastonite contents in glasses i.e. W-10 (corresponds to 10% wollastonite), W-20 (corresponds to 20% wollastonite), etc. High purity powders of $SiO_2$ (purity > 99.5%), $CaCO_3$ (>99.5%), $MgCO_3$ (BDH Chemicals Ltd., UK, purity > 99.0%), $NH_4H_2PO_4$ (Sigma–Aldrich, Germany, >99.0%) and $CaF_2$ (Sigma–Aldrich, Germany, 325 mesh, >99.9%) were used. Homogeneous mixtures of batches (∼100 g), obtained by ball milling, were preheated at 900 °C for 1 h for calcination and then melted in Pt crucibles at 1590 °C for 1–2 h, depending on glass composition. The glasses were obtained in frit form by quenching of glass melts in cold water while the monolithic glasses were obtained by pouring of glass melt on a metallic mould and annealing at 500 °C for 1 h. The dried frits were milled to achieve fine glass powders with mean particle sizes of ∼10–20 μm (determined by light scattering technique; Coulter LS 230, Beckman Coulter, Fullerton CA; Fraunhofer optical model). The amorphous nature of glasses was confirmed by X-ray diffraction (XRD) analysis (Rigaku Geigerflex D/Max, Tokyo, Japan; C Series; Cu-$K_\alpha$ radiation; 2$\theta$ angle range 10–60°; step 0.02° $s^{-1}$).

### 2.2. Structural characterization

#### 2.2.1. Infrared spectroscopy

Infrared spectra of the glasses were obtained using an Infrared Fourier spectrometer (FTIR, model Mattson Galaxy S-7000, USA). For this purpose glass powders were mixed with KBr in the proportion of 1/150 (by weight) and pressed into a pellet using a hand press. 64 scans for background and 64 scans per sample were made with signal gain 1. The resolution was 4 $cm^{-1}$.

#### 2.2.2. Magic angle spinning (MAS)-nuclear magnetic resonance (NMR) spectroscopy

The $^{29}Si$ MAS-NMR spectra were recorded on a Bruker ASX 400 spectrometer operating at 79.52 MHz (9.4 T) using a 7 mm probe at a spinning rate of 5 kHz. The pulse length was 2 μs and 60 s delay time was used. Kaolinite was used as the chemical shift reference. The $^{31}P$ MAS-NMR spectra of glasses were recorded on a Bruker ASX 400 spectrometer operating at 161.97 MHz with 45° pulses, spinning rates of 12 kHz, a 60 s recycle delay and the chemical shift was quoted in ppm from phosphoric acid (85%).

### 2.3. Thermal analysis

The differential thermal analysis (DTA-TG, Setaram Labsys, Setaram Instrumentation, Caluire, France) of glass powders was carried out in air from room temperature to 1000 °C at different heating rates ($\beta$) of 10 K $min^{-1}$. The glass powders (mean particle size: 10–20 μm) weighing 50 mg were contained in an alumina crucible and the reference material was α-alumina powder.

### 2.4. Crystallization of glass powder compacts

Round shaped pellets with 20 mm diameter and ∼3 mm thickness were prepared from fine glass powder by uniaxial pressing (80 MPa). The samples were sintered under non-isothermal conditions ($\beta$ = 5 K $min^{-1}$) at 850 °C for 1 h in a box furnace in air.

Table 1
Composition of glasses.

| Glass | | CaO | MgO | $SiO_2$ | $P_2O_5$ | $CaF_2$ |
|---|---|---|---|---|---|---|
| W-10 | Wt.% | 32.96 | 13.03 | 44.02 | 8.44 | 1.55 |
| | Mol.% | 34.12 | 18.76 | 42.52 | 3.45 | 1.15 |
| W-20 | Wt.% | 35.20 | 11.17 | 43.64 | 8.44 | 1.55 |
| | Mol.% | 36.70 | 16.20 | 42.46 | 3.48 | 1.16 |
| W-30 | Wt.% | 37.44 | 9.31 | 43.26 | 8.44 | 1.55 |
| | Mol.% | 39.32 | 13.60 | 42.41 | 3.50 | 1.17 |
| W-40 | Wt.% | 39.68 | 7.44 | 42.89 | 8.44 | 1.55 |
| | Mol.% | 39.68 | 10.96 | 42.35 | 3.53 | 1.18 |
| W-50 | Wt.% | 41.91 | 5.58 | 42.51 | 8.44 | 1.55 |
| | Mol.% | 44.68 | 8.28 | 42.29 | 3.56 | 1.19 |
| W-60 | Wt.% | 44.15 | 3.72 | 42.13 | 8.44 | 1.55 |
| | Mol.% | 47.42 | 5.56 | 42.24 | 3.58 | 1.19 |
| W-70 | Wt.% | 46.39 | 1.86 | 41.76 | 8.44 | 1.55 |
| | Mol.% | 50.21 | 2.80 | 42.18 | 3.61 | 1.20 |
| W-80 | Wt.% | 48.63 | 0.00 | 41.38 | 8.44 | 1.55 |
| | Mol.% | 53.03 | 0.00 | 42.12 | 3.64 | 1.21 |

### 2.5. Crystalline phase analysis and microstructure of glass–ceramics

The qualitative and quantitative analysis of crystalline phases in the glass–ceramics (crushed to particle size <63 μm) were determined by XRD analysis using a conventional Bragg-Brentano diffractometer (Philips PW 3710, Eindhoven, The Netherlands) with Ni-filtered Cu-$K_\alpha$ radiation. The quantitative phase analysis of the glass–ceramics was made by combined Rietveld-R.I.R (reference intensity ratio) method. A 10 wt.% of corundum (NIST SRM 676a) was added to all the glass–ceramic samples as an internal standard. The mixtures, ground in an agate mortar, were side loaded in aluminium flat holder in order to minimize the preferred orientation problems. Data were recorded in $2\theta$ range = 5–115° (step size 0.02° and 50 s of counting time for each step). The phase fractions were extracted by Rietveld-R.I.R refinements using the software TOPAS 3 (Bruker AXS, Karlsruhe, Germany) and were rescaled on the basis of the absolute weight of corundum originally added to their mixtures as an internal standard, and therefore, internally renormalized.

Microstructural observations were done on polished (mirror finishing) glass–ceramics, and from the surface of unpolished glasses. The as obtained glass and the etched glass–ceramic samples (by immersion in 2 vol.% HF solution for a duration of 2 min and washing with distilled water in order to stop the etching process and avoid the fluorides formation) were observed by scanning electron microscopy (SEM; SU-70, Hitachi) with energy dispersive spectroscopy (EDS; Bruker Quantax, Germany) to study the distribution of elements in the crystals.

## 3. Results and discussion

### 3.1. Structure of glasses

The bioactive properties of phosphosilicate glasses depend on the presence of large amounts of network modifying cations, whose charge balance is achieved by breaking Si–O–Si bridges and creating corresponding high concentrations of nonbridging oxygen (NBO) atoms, and thus a significant fragmentation of the silicate network. Indeed, experimental[16] and simulation data[17] show that the bulk structure of common melt-derived bioactive compositions is dominated by interconnected chains of $Q^2$ silicate tetrahedra [$Q^n$ notation denotes a tetrahedron with n bridging oxygens (BOs)] and predominantly isolated phosphate groups. Therefore, undoubtedly, the molecular structure of glasses plays a crucial role in deciding their bioactivity and understanding these details allows designing new glasses with improved chemical durability and tailored biodegradability for specific applications.

Magnesium is involved in over 300 chemical reactions in the body and is known to activate phagocytosis and regulate active calcium transport.[18] It is due to this reason that it has been often incorporated into bioactive glasses.[5,19–25] However, the structural role of magnesium in bioactive glasses is still ambiguous owing to the lack of information on its local environment. For example: MgO is considered to behave like CaO (i.e. network modifier), within a silicate glass structure but its elemental properties such as charge to size ratio and Pauling electronegativity suggest that $Mg^{2+}$ falls on the boundary between being a network modifier and an intermediate oxide. Also, there are evidences which exhibit that MgO may act as intermediate oxide in highly disrupted silicate glasses from the extension of the glass forming region in ternary diagrams towards lower $SiO_2$ mole fractions.[26] Similar observations have been reported by Watts et al.[27]

In the present study, the room temperature FTIR transmittance spectra of all the investigated glasses (Fig. 1) exhibit three broad transmittance bands in the region of 300–1500 $cm^{-1}$. This lack of sharp features is indicative of the general disorder in the silicate and phosphate network mainly due to a wide distribution of $Q^n$ units occurring in these glasses. The most intense bands in the 800–1300 $cm^{-1}$ region correspond to the stretching vibrations of the $SiO_4$ tetrahedron with a different number of bridging oxygen atoms.[28] Further, in all the glasses, this region (i.e. 800–1300 $cm^{-1}$) is split in two transmittance bands centred at ~1040 $cm^{-1}$ and ~920 $cm^{-1}$. The high frequency band

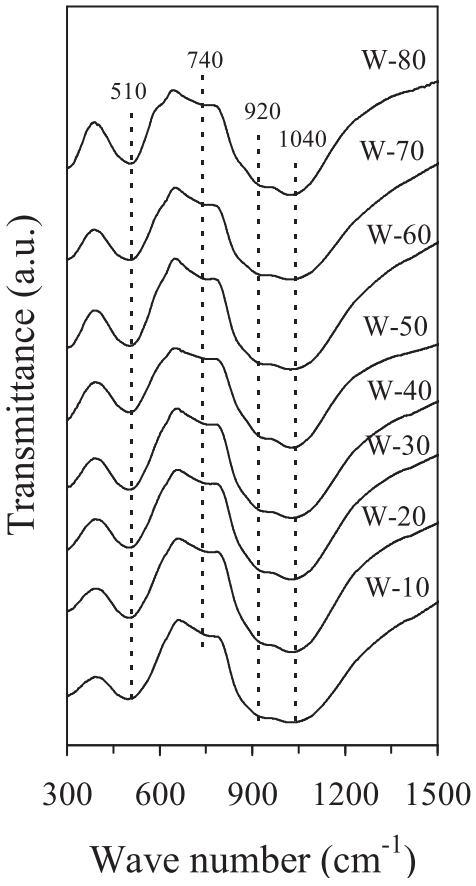


Fig. 1. FTIR spectra of the investigated glasses.

can be assigned to the Si–O asymmetric stretching mode of BOs, whereas the ~920 $cm^{-1}$ may be attributed to the Si–O asymmetric stretching mode of the non-bridging oxygens (NBOs).[29,30] Furthermore, the 510 $cm^{-1}$ band can be attributed to Si–O–Si bending modes,[29] while the weak 740 $cm^{-1}$ shoulder may be due to Si–O–Si symmetric stretching with simultaneous Si cation motions.[31] It is noteworthy that the high frequency band at 1040 $cm^{-1}$ may also be assigned to the asymmetric stretching of $PO_4$ units which has been reported to appear in crystalline fluorapatite at 1038 $cm^{-1}$.[32] No significant differences in the infrared spectra of the investigated glasses could be observed thus depicting that varying CaO/MgO ratio in glasses did not affect the structure of glasses substantially.

In agreement with FTIR studies, the $^{29}$Si MAS-NMR spectra for all the investigated glasses (Fig. 2a) depict the dominance of $Q^2$ (Si) structural units in the glasses.[16] Further, only slight shift in the peak positions of spectra could be observed and all the spectra are centred between −82.2 ppm and −82.9 ppm, thus depicting no significant changes in the silicon coordination in glass structure. Similar results have been reported by Galliano et al.[33] where it has been shown that the type and distribution of silicate units in an alkaline-earth phosphosilicate glass does not depend on the nature of the alkaline-earth cations present in the system. It has been well documented in literature[34] that depending on the glass composition and experimental techniques employed to synthesize the glass, Mg has been found to

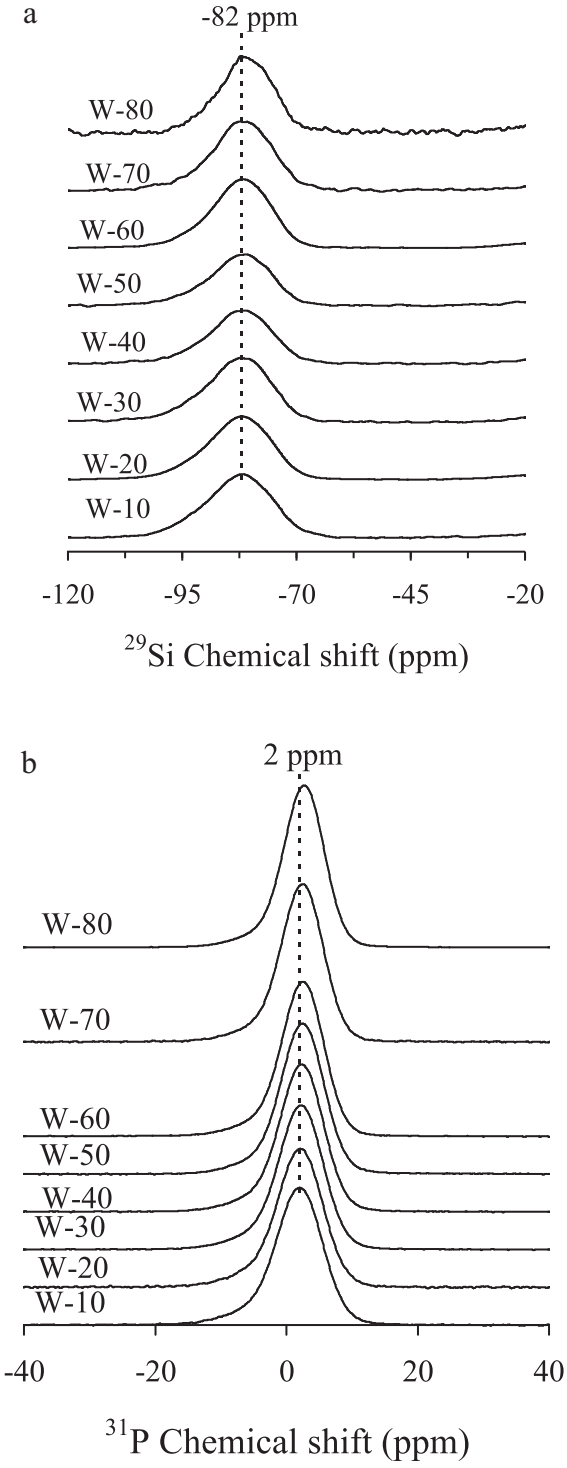


Fig. 2. (a) $^{29}$Si MAS-NMR spectra and (b) $^{31}$P MAS-NMR spectra of investigated glasses.

exist in 4–5- and 6-fold coordination. Recently, Pedone et al.[34] studied the influence of varying CaO/MgO ratio on the structure of 45S5 Bioglass® using computation models and discussed its further implications on the bioactivity of the glass. It was concluded that varying CaO/MgO ratio does not affect the overall network connectivity of the glass and the number of NBOs remain unchanged; although, the higher field strength of Mg with

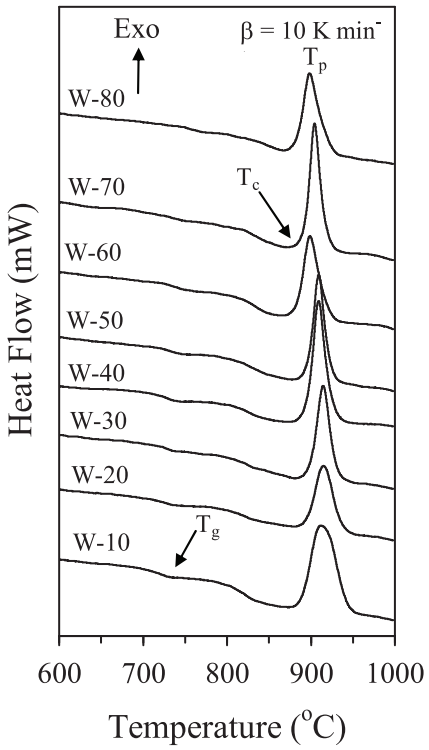


Fig. 3. DTA thermographs of the investigated glasses at heating rate 10 K min$^{-1}$.

respect to Ca provides for the former a sufficient driving force to rearrange the $SiO_4$ tetrahedra in such a way that only NBOs belonging to different tetrahedral coordinate with Mg ions.

The $^{31}$P MAS-NMR spectra of all the glasses show a predominance of an orthophosphate-type environment (Fig. 1b). In fact, the observed chemical shifts, 1–3 ppm, are close to that of the calcium orthophosphate (3.1 ppm) and that of the amorphous magnesium orthophosphate (*ca.* 0.5 ppm).[16] These results are in good co-relation with those reported by Lusvardi et al.[35] and Linati e al.[36] for the 45S5 glass where it has been deduced a fraction of orthophosphate units of ~82% while the rest might be comprised meta- or pyrophosphates. Furthermore, the presence of fluorine in the phospho-silicate glass network is known to induce significant changes in the local oxygen environment since the donor ability of fluoride is weaker in comparison to oxide, making the possibility of Si–F formation, unlikely. Therefore, under such conditions, fluoride remains predominantly in ionic state and prefers to form ionic bonds with metal cations (Ca and Mg in present study), thus avoiding the de-polymerization of silicate glass network and forcing phosphate groups to link with silicate groups, leading to higher glass connectivity,[35] which might hamper their bioactivity. However, it is noteworthy that, in the present case, the possibility of formation Si–O–P bonds is low if not negligible. In fact, according to the NMR results, phosphate groups are not part of the actual glass network backbone.

### 3.2. Thermal behaviour of glasses

The DTA plots of glass powders, shown in Fig. 3, feature an endothermic dip corresponding to glass transition temperature

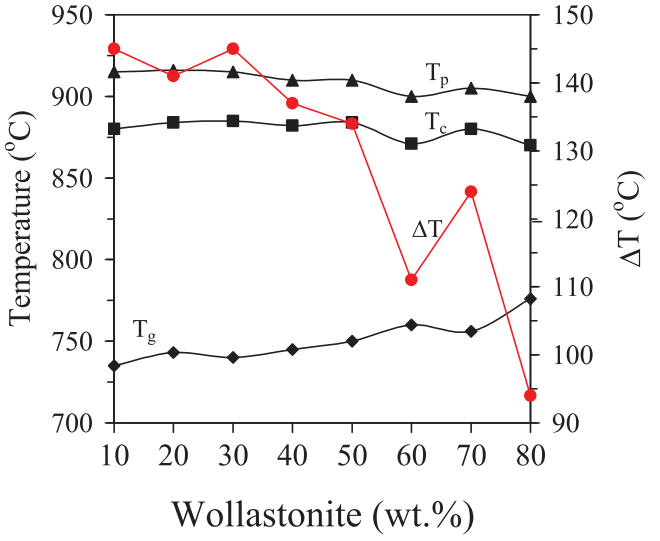


Fig. 4. Influence of CaO/MgO ratio (wollastonite content) on different thermal parameters of glasses as obtained from DTA.

($T_g$) before the onset of crystallization ($T_c$) and a well-defined single exothermic crystallization curve. The presence of single crystallization exotherm anticipates that the glass–ceramic is formed either as a result of single phase crystallization or of an almost simultaneous precipitation of different crystalline phases. Fig. 4 and Table 2 present the variation in $T_g$, $T_c$ and peak temperature of crystallization ($T_p$) with increasing wollastonite content in glasses (or increasing CaO/MgO ratio in glasses). On an average, $T_g$ shifted towards higher values with increasing CaO/MgO ratio in glasses. Although, the Si $Q^n$ distribution of the investigated glasses is very similar, it has been reported that varying CaO/MgO ratio drastically affects the topology of rings in glasses.[34] This trend may be explained on the basis of higher field strength of MgO due to which the replacement of $Mg^{2+}$ by $Ca^{2+}$ favours the formation of smaller rings in silica matrix thus, affecting the connectivity between the $SiO_4$ tetrahedra. This is also a key feature for lowering melt viscosities of Mg-containing silicate glasses.[37] Further, no significant variations in the values of $T_c$ (880 ± 6 °C) and $T_p$ (809 ± 6 °C) were observed with varying CaO/MgO ratio in glasses (Fig. 4).

With respect to the sintering ability of glasses, Fig. 4 presents the variation in thermal stability parameter $\Delta T$ (= $T_c - T_g$) for all the investigated glasses. The higher values of $\Delta T$ correspond to delay in nucleation and thus, provide wider processing window

Table 2
Thermal parameters (°C) of glasses as obtained from DTA.

| Glass | $T_g$ | $T_c$ | $T_p$ | $\Delta T$ |
|---|---|---|---|---|
| W-10 | 735 | 880 | 915 | 145 |
| W-20 | 743 | 884 | 916 | 141 |
| W-30 | 740 | 885 | 915 | 145 |
| W-40 | 745 | 882 | 910 | 137 |
| W-50 | 750 | 884 | 910 | 134 |
| W-60 | 760 | 871 | 900 | 111 |
| W-70 | 756 | 880 | 905 | 124 |
| W-80 | 776 | 870 | 900 | 94 |

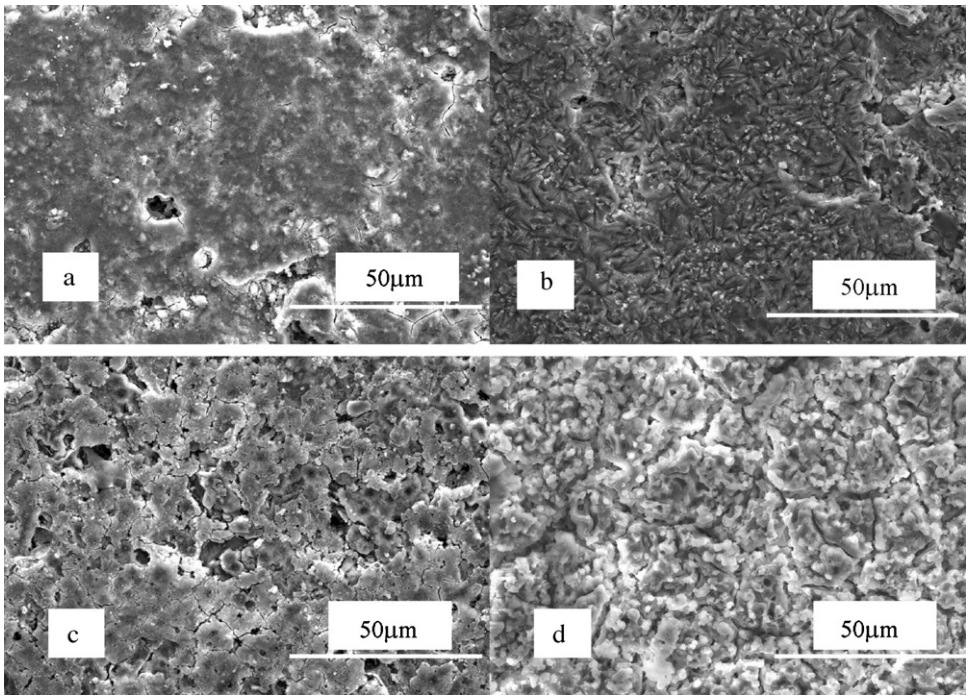


Fig. 5. SEM images of glass–ceramics (a) W-10, (b) W-20, (c) W-70 and (d) W-80 after sintering at 850 °C for 1 h.

for a glass composition to attain maximum densification. In the present study, increasing calcium content in glasses decreases the value of $\Delta T$, thus implying towards degradation in sintering behaviour of glasses. However, in any case, the value of $\Delta T$ obtained for all the investigated glasses is high enough to help the glass powders attain good densification during sintering. These observations are in good agreement with the results of Karamanov and Pelino[38] where it has been reported that wollastonite based glass–ceramics possess lower mechanical strength in comparison to diopside based glass–ceramics. It is worth mentioning that the detailed analysis of mechanical properties of the investigated GCs will be presented in our forthcoming article.

In accordance with DTA results, well sintered glass–ceramics were obtained after sintering of glass powders at 850 °C for 1 h. As is evident from Fig. 6, the XRD results reveal the presence of diopside ($CaMgSi_2O_6$; ICDD card: 01-078-1390), fluorapatite [$Ca_5(PO_4)_3F$; ICSD: 01-071-3848], wollastonite 2 M ($CaSiO_3$; ICSD: 20589) and pseudowollastonite ($CaSiO_3$; ICSD: 87694) as the only crystalline phases in all the glass–ceramics except composition W-80 which is free from diopside. Fig. 7 presents the quantitative analysis of variation in crystalline/amorphous content in all the investigated glass–ceramics with respect to their wollastonite content while Fig. 8 shows the fit of a measured XRD pattern of a sintered glass–ceramic by using the TOPAS software. The fitting to the measured X-ray diagram has been performed by a least-square calculation. The calculated diagram (Fig. 8) is based on crystallographic structure models, which also take into account specific instrument and sample effects. The parameters of this model have been refined simultaneously using least-squares methods in order to obtain the best fit to all measured data. The difference plot in Fig. 8 does not show any significant misfits. The differences between the main peaks of diopside, fluorapatite, wollastonite and pseudowollastonite are caused by adjustment difficulties based on the crystallinity of the phases.

As is evident from Fig. 8, the starting glass composition (W-10) comprises mainly of residual amorphous glassy phase (∼60 wt.%) which decreased with increasing CaO/MgO ratio in glasses until glass composition W-50 while further increase in CaO/MgO ratio in glasses again led to an increase in

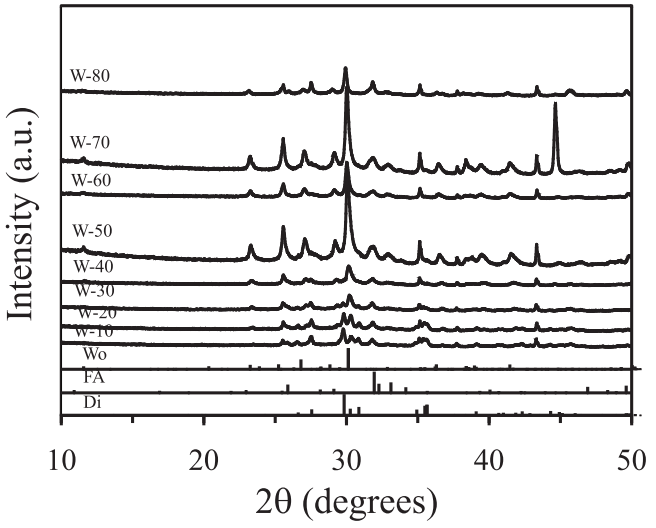


Fig. 6. X-ray diffractograms of glass powder compacts after sintering at 850 °C for 1 h. 10 wt.% corundum ($Al_2O_3$) has been added in the glass–ceramic powders as an internal standard for quantitative analysis. The phase reflections corresponding to $Al_2O_3$ have not been marked. Also, phase reflections corresponding to pseudowollastonite ($CaSiO_3$; ICSD: 87694) have not be marked as we could not obtain a PDF card for the same.

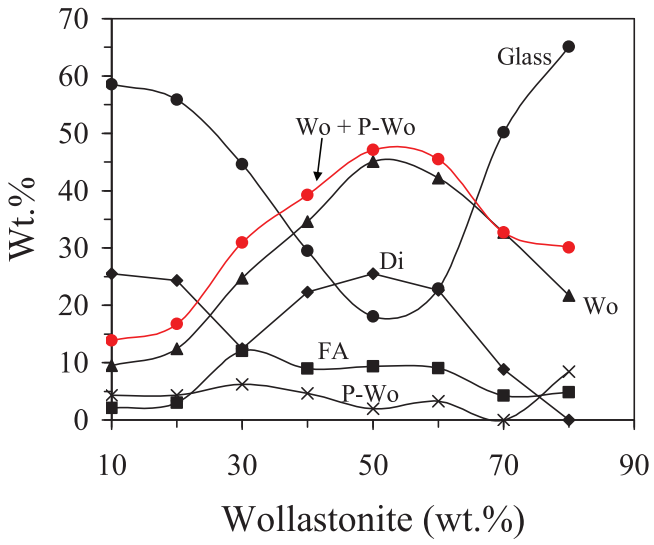


Fig. 7. Plot depicting the variation in crystalline/amorphous ratio of glass–ceramics with respect to CaO/MgO ratio (wollastonite content) as calculated from Rietveld refinement of XRD data.

amorphous content in glass–ceramics. The residual glassy phase in glass–ceramics is of crucial importance as it controls the apatite forming ability of glass–ceramics[39,40] and the glass–ceramic may turn bio-inert if residual glassy phase is in low amount (<5 wt.%). Thus, the design of glass–ceramic compositions needs to be such that equilibrium is achieved in the midst of biological and mechanical properties of the final material. In the present investigation, the amount of residual glassy phase is high enough to render good bioactivity to resultant GC material.

The microstructure of glass–ceramics as observed by SEM (Fig. 5) is in good agreement with XRD results. The SEM images of glass–ceramics W-10 and W-20 exhibit highly dense microstructure (Fig. 5a and b) implying towards good sintering behaviour of glass–ceramics. Although, the glass–ceramic compositions W-70 and W-80 possess almost similar or even higher amount of residual glassy phase than W-10, still the degradation in sintering ability of these glass compositions may be attributed to the variation in the amount of porosity in these glass–ceramics owing to their different nature and amount of crystalline content. According to Karamanov and Pelino,[38] both diopside as well as wollastonite based glass–ceramics possess good sintering ability. However, due to crystallization volume fraction of diopside and wollastonite, intragranular crystallization induced porosity is formed in these glass–ceramics which affects the sintering ability of these glass–ceramics, thus resulting in poor mechanical strength of wollastonite based compositions. This explanation is concurrent with the microstructure of glass–ceramics W-70 (Fig. 5c) and W-80 (Fig. 5d), respectively.

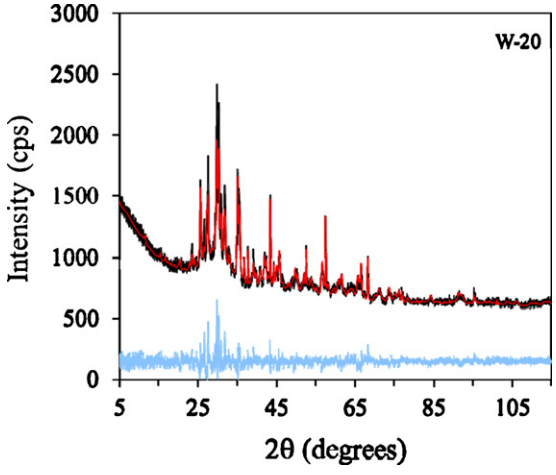


Fig. 8. Observed (black), calculated (red) and difference (blue) curves from the Rietveld refinement of GC W-20. (For interpretation of the references to color in this figure legend, the reader is referred to the web version of this article.)

## 4. Conclusions

The influence of varying CaO/MgO ratio on the structure, sintering and crystallization behaviour of diopside–fluorapatite–wollastonite based glasses and glass–ceramics has been investigated. The variation in CaO/MgO ratio on glasses did not exhibit any significant effect on the structure of glasses with Si predominantly present in $Q^2$ units while phosphate is coordinated in orthophosphate environment. With respect to thermal behaviour of glasses, heat treatment of glass powders at 850 °C for 1 h resulted in well sintered glass–ceramics with diopside, fluorapatite, wollastonite and pseudowollastonite as the crystalline phases. Increasing CaO/MgO ratio in glasses degraded their sintering behaviour and resulted in different amorphous/crystalline ratio in resultant glass–ceramics with the glass–ceramic W-10 and W-80 exhibiting the highest amount of residual glassy phase which is appropriate for a material to show good bioactivity.

It should be mentioned here that it is crucial to analyze the bioactive behaviour and mechanical properties of these glass–ceramics so as to prove their efficacy as potential materials for application in human biomedicine. This will form the basis of our forthcoming study.

## Acknowledgements

Ishu Kansal is thankful to FCT-Portugal for her doctoral research grant. The support of University of Aveiro and CICECO is highly appreciated.

## References

1. Hench LL, et al. Bonding mechanisms at the interface of ceramic prosthetic materials. *Journal of Biomedical Materials Research* 1971;**5**(6): 117–41.
2. Hench LL. Bioactive ceramics: theory and clinical applications. In: Anderson OH, Yli-Urpo A, editors. *Bioceramics 7*. Oxford, UK: Butterworth-Heinemann; 1994.
3. Langer R, Vacanti JP. Tissue engineering. *Science* 1993;**260**(5110):920–6.
4. Hollister SJ. Porous scaffold design for tissue engineering. *Nature Materials* 2005;**4**(7):518–24.
5. Kansal I, Tulyaganov DU, Goel A, Pascual MJ, Ferreira JMF. Structural analysis and thermal behavior of diopside–fluorapatite–wollastonite-based glasses and glass–ceramics. *Acta Biomaterialia* 2010;**6**(11):4380–8.

6. Kokubo T. Bioactive glass ceramics: properties and applications. *Biomaterials* 1991;**12**(2):155–63.
7. Vitale-Brovarone C, Verné E, Robiglio L, Appendino P, Bassi F, Martinasso G, Muzio G, Canuto R. Development of glass–ceramic scaffolds for bone tissue engineering: characterisation, proliferation of human osteoblasts and nodule formation. *Acta Biomaterialia* 2007;**3**(2):199–208.
8. Renghini C, Komlev V, Fiori F, Verné E, Baino F, Vitale-Brovarone C. Micro-CT studies on 3-D bioactive glass–ceramic scaffolds for bone regeneration. *Acta Biomaterialia* 2009;**5**(4):1328–37.
9. Shibuya T, Morita Y, Matsui A. *No alkali containing biocompatible glass–ceramic with apatite, wollastonite and diopside crystals mixed*. United States: U. Patent, Editor; 1988.
10. Salman SM, Salama SN, Darwish H, Abo-Mosallam HA. In vitro bioactivity of glass–ceramics of the $CaMgSi_2O_6$–$CaSiO_3$–$Ca_5(PO_4)_3F$–$Na_2SiO_3$ system with $TiO_2$ or ZnO additives. *Ceramics International* 2009;**35**(3):1083–93.
11. Kansal I, Goel A, Tulyaganov DU, Santos LF, Ferreira JMF. Diopside (CaO MgO $2SiO_2$)–fluorapatite (9CaO $3P_2O_5$ $CaF_2$) glass–ceramics: Potential materials for bone tissue engineering. *Journal of Materials Chemistry* 2011;**21**:16247–56.
12. Wu C, Ramaswamy Y, Zreiqat H. Porous diopside (CaMgSi(2)O(6)) scaffold: a promising bioactive material for bone tissue engineering. *Acta Biomaterialia* 2010;**6**(6):2237–45.
13. Wu C, Zreiqat H. Porous bioactive diopside (CaMgSi(2)O(6)) ceramic microspheres for drug delivery. *Acta Biomaterialia* 2010;**6**(3):820–9.
14. Zhang N, Molenda JA, Fournelle JH, Murphy WL, Sahai N. Effects of pseudowollastonite ($CaSiO_3$) bioceramic on in vitro activity of human mesenchymal stem cells. *Biomaterials* 2010;**31**(30):7653–65.
15. Sainz MA, Pena P, Serena S, Caballero A. Influence of design on bioactivity of novel $CaSiO_3$–$CaMg(SiO_3)_2$ bioceramics: in vitro simulated body fluid test and thermodynamic simulation. *Acta Biomaterialia* 2010;**6**(7):2797–807.
16. Brauer DS, Karpukhina N, Law RV, Hill RG. Structure of fluoride-containing bioactive glasses. *Journal of Materials Chemistry* 2009;**19**(31):5629–36.
17. Tilocca A. Structural models of bioactive glasses from molecular dynamics simulations. *Proceedings of the Royal Society A – Mathematical Physical and Engineering Sciences* 2009;**465**(2104):1003–27.
18. Saris NEL, Mervaala E, Karppanen H, Khawaja JA, Lewenstam A. Magnesium – an update on physiological, clinical and analytical aspects. *Clinica Chimica Acta* 2000;**294**(1–2):1–26.
19. Jallot E. Role of magnesium during spontaneous formation of a calcium phosphate layer at the periphery of a bioactive glass coating doped with MgO. *Applied Surface Science* 2003;**211**(1–4):89–95.
20. Hesaraki S, Safari M, Shokrgozar MA. Composite bone substitute materials based on beta-tricalcium phosphate and magnesium-containing sol–gel derived bioactive glass. *Journal of Materials Science – Materials in Medicine* 2009;**20**(10):2011–7.
21. Ma J, Chena CZ, Wanga DG, Hu JH. Synthesis: characterization and in vitro bioactivity of magnesium-doped sol–gel glass and glass–ceramics. *Ceramics International* 2011;**37**(5):1637–44.
22. Amaoka E, Vedel E, Nakamura S, Moriyoshi Y, Salonen JI, Yamashita K. Effect of electrical polarization on the behavior of bioactive glass containing MgO and $B_2O_3$ in SBF. *Bioceramics* 2006;**18**(Pts. 1 and 2), 309–311, 333–336.
23. Hashmi MU, Shah SA, Alam S, Shamim A. Dissolution behavior of bioactive glass ceramics with different CaO/MgO ratios. *Ceramics-Silikaty* 2010;**54**(1):8–13.
24. Kokubo T, Ito S, Sakka S, Yamamuro T. Formation of a high-strength bioactive glass ceramic in the system MgO–CaO–$SiO_2$–$P_2O_5$. *Journal of Materials Science* 1986;**21**(2):536–40.
25. Radev L, Hristov V, Michailova I, Samuneva B. Sol–gel bioactive glass–ceramics part II: glass–ceramics in the CaO–SiO(2)–P(2)O(5)–MgO system. *Central European Journal of Chemistry* 2009;**7**(3):322–7.
26. McMillan PW. *Gass ceramics*. London: Academic Press; 1979.
27. Watts SJ, Hill RG, O'Donnell MD, Law RV. Influence of magnesia on the structure and properties of bioactive glasses. *Journal of Non-Crystalline Solids* 2010;**356**(9–10):517–24.
28. Stoch L, Sroda M. Infrared spectroscopy in the investigation of oxide glasses structure. *Journal of Molecular Structure* 1999;**511–512**:77–84.
29. Omori K. Analysis of infrared absorption spectrum of diopside. *American Mineralogist* 1971;**56**(9–10):1607.
30. Aronne A, Sigaev VN, Champagnon B, Fanelli E, Califano V, Usmanova LZ, Pernice P. The origin of nanostructuring in potassium niobiosilicate glasses by Raman and FTIR spectroscopy. *Journal of Non-Crystalline Solids* 2005;**351**(46–48):3610–8.
31. Galeener FL. Theory of 2nd order vibrational-spectra of molecular glasses. *Bulletin of the American Physical Society* 1976;**21**(3):369.
32. Williams Q, Knittle E. Infrared and Raman spectra of Ca-5(PO4)(3)F-2-fluorapatite at high pressures: compression-induced changes in phosphate site and Davydov splittings. *Journal of Physics and Chemistry of Solids* 1996;**57**(4):417–22.
33. Galliano PG, Lopez JMP, Varetti EL, Sobrados I, Sanz J. Analysis by nuclear-magnetic-resonance and Raman spectroscopies of the structure of bioactive alkaline-earth silicophosphate glasses. *Materials Research Bulletin* 1994;**29**(12):1297–306.
34. Menziani MC, Pedone A, Malavasi G. Computational insight into the effect of CaO/MgO substitution on the structural properties of phospho-silicate bioactive glasses. *Journal of Physical Chemistry C* 2009;**113**(35):15723–30.
35. Lusvardi G, Malavasi G, Cortada M, Menabue L, Menziani MC, Pedone A, Segre U. Elucidation of the structural role of fluorine in potentially bioactive glasses by experimental and computational investigation. *Journal of Physical Chemistry B* 2008;**112**(40):12730–9.
36. Linati L, Lusvardi G, Malavasi G, Menabue L, Menziani MC, Mustarelli P, Pedone A, Segre U. Medium-range order in phospho-silicate bioactive glasses: insights from MAS-NMR spectra, chemical durability experiments and molecular dynamics simulations. *Journal of Non-Crystalline Solids* 2008;**354**(2–9):84–9.
37. Wilantewicz T. *The effects of lithium, boron and magnesium oxides on the mechanical properties of silicate glasses*. New York: Alfred University; 1998.
38. Karamanov A, Pelino M. Induced crystallization porosity and properties of sintereds diopside and wollastonite glass–ceramics. *Journal of the European Ceramic Society* 2008;**28**(3):555–62.
39. Strnad Z. Role of the glass phase in bioactive glass–ceramics. *Biomaterials* 1992;**13**(5):317–21.
40. Li P, Yang Q, Zhang F, Kokubo T. The effect of residual glassy phase in a bioactive glass–ceramic on the formation of its surface apatite layer. *Journal of Materials Science: Materials in Medicine* 1992;**3**(6):452–6.